Int. J. Electrochem. Sci., 13 **(2018)** 2299 – 2309, doi: 10.20964/2018.03.59

International Journal of
ELECTROCHEMICAL
SCIENCE
www.electrochemsci.org

Synthesis of Au-modified Reduced Graphene Oxide Supported Pd-Ni nanocomposites and electrocatalytic activity for propane-1,3-diol oxidation

Xudong Huang[1], *Tianci Niu*[2], *Yujie Shi*[3], *Yan Jiang*[*]

Jiangsu Key Laboratory of Advanced Catalytic Materials and Technology, Changzhou University, Jiangsu 213164, People's Republic of China
[*]E-mail: jy@cczu.edu.cn

Received: 6 November 2017 / *Accepted:* 5 January 2018 / *Published:* 5 February 2018

A Reduced Graphene Oxide-Supported Pd-Ni nanocomposite **(**Pd_1Ni_4/RGO) was prepared by simultaneous chemical reduction, on the surface of which a small amount of Au nanoparticles were subsequently deposited via potentiontatic deposition to obtain an Au-deposited Pd_1Ni_4/RGO (denoted as $Au_{(x)}$-Pd_1Ni_4/RGO, x = 1, 2, and 5 s, representing the deposition time of Au). As a representative, the surface structure of the $Au_{(1s)}$-Pd_1Ni_4/RGO electrode was characterized and analyzed by scanning electron microscopy (SEM), transmission electron microscopy (TEM), energy dispersive X-ray spectrum (EDX) and X-ray diffraction (XRD), respectively. The modification approach described here is simple, effective and versatile, which can be further used to modify other metal substrates with an additional metal. Moreover, the Au deposition induces a positive effect on the electro-catalytic activity for propane-1,3-diol oxidation in alkaline media in comparison to the Pd_1Ni_4/RGO.

Keywords: nanocomposite; electrocatalytic activity; electrode; catalyseis.

1. INTRODUCTION

Recently, multi-metallic catalysts were extensively studied due to the so-called "synergistic effect" that can lead to increased activity and thus lower catalyst loading. In a series of studies on electro-catalytic oxidation of alcohols, precious metals (Au, Pt and Pd) were mainly found as the active sites [1]. As Pd is relatively more abundant and less expensive than Pt and Au, it was the most extensively studied one [2-4], and Pd-M′ (M′: transition metal) type bi-metallic catalysts are attracting increasing attention. Pd-Au bi-metallic nanostructure is one of the well-explored systems, which was generally prepared through co-depositing Pd and Au in a solution containing their precursors by

chemical reduction method [15-19]. Loading Pd-Au nanoparticles on appropriate supports could further enhance the catalytic activity for alcohol oxidation [20]. However, it has limited practical value considering the high cost of the two precious metals.

Nickel represents one of the inexpensive transition metals, which has been extensively used in the domain of Ni-metal hydride rechargeable battery and electroplating [5, 6]. Compared to bulk nickel electrode, it is more active in alcohol oxidation when deposited on graphite or glassy carbon substrates [7, 8]. Moreover, research has shown that the activity could be significantly improved when it was co-deposited with a second nucleus such as Pd or Au [9-14]. We therefore postulate that the combination of Pd, Au with Ni to generate a tri-metallic composite will be of great potential [21].

In the last few years, polyols have received increasing attention as potential fuel cells in addition to monohydric alcohols such as ethanol and methanol. The electrochemical oxidation of glycol and glycerol on different electro-catalysts has been well studied [22-24]. Propane-1,3-diol containing two hydroxyl groups, on the other hand, is less investigated yet more valuable due to its the higher chemical energy/electric conversion rate [25].

As our contribution, we herein report the preparation of an Au deposited Pd_1Ni_4/RGO via simultaneous chemical reduction and electron-chemical deposition. The tri-metallic composite material was characterized by SEM and TEM, and its electro-catalytic performance in propane-1,3-diol oxidation was studied.

2. EXPERIMENTAL

2.1 Synthesis of Pd_1Ni_4/RGO Composites

Graphite oxide (GO) was prepared by oxidization of graphite flake according to the modified Hummer's method [26, 27]. Then, 5 mL of 0.4 mg mL^{-1} GO was added to 15 mL of the second distilled water solution which containing 58.6 μL of 0.1 mol L^{-1} Ni $(NO_3)_2$ and 735 μL of 2 mmol L^{-1} Pd $(NO_3)_2$. After sonicating the mixture for 40 minutes, added 30 mg of $NaBH_4$ to the mixture with stirring. The reduction was carried out for 2 h at room temperature to obtain the Pd-Ni nanoparticles and reduced graphene oxide (RGO). After the formed Pd-Ni nanoparticles supported RGO (Pd_1Ni_4/RGO) precipitation over the night, the supernatant was removed to get 1 mL of residue. Next, the obtained residue was sonificated to form a homogeneous black suspension. The glassy carbon electrodes (GCE) with diameter of 4 mm were sequentially polished with alumina powders with particle diameters of 0.35 μm and 0.05 μm. Then, the electrodes were subjected to ultrasonic washing in distilled water, absolute ethanol, and twice distilled water, respectively. Next, 5 μL of the above suspension was dropped onto the surface of a clean GCE. The prepared catalyst (Pd1Ni4/RGO) modified glassy carbon electrode as the working electrode for the deposition of Au, and then allowed to dry in air for other electrochemical measurements. The total mass of Pd and Ni loading of Pd_1Ni_4/RGO was about 44 μg cm^{-2} on the part of the surface area of GCE. The Pd_1Ni_4/RGO-supported Au nanoparticles ($Au_{(x)}$-Pd_1Ni_4/RGO) modified GCE was also prepared by using $HAuCl_4$ (a precursor of Au).

2.2 Electrochemical Measurements

Pd_1Ni_4/RGO modified glassy carbon electrode (GCE) as the working electrode, a platinum foil (10 × 5 mm) as the counter electrode and a KCl saturated calomel electrode (SCE) as the reference electrode, respectively. The electrochemical experiments were performed with a LK98BII (Lanlike Ltd.) electrochemical analyzer. In a typical procedure, a positive potential of +0.60 V vs. SCE for a desired time was exerted on the GCE for the depositon of Au on Pd_1Ni_4/RGO was prepared in 0.05 mol L^{-1} H_2SO_4 solution containing 1mmol L^{-1} $HAuCl_4$. Next, the Au-deposited Pd_1Ni_4/RGO (Au-Pd_1Ni_4/RGO) was taken out of the solution, and then washed with water to electrochemical measurements and characterization. $Au_{(x)}$-Pd_1Ni_4/RGO (where X represents the modification time of Au) catalysts with different Au loadings were prepared by changing the Au deposition time. In this paper, the modification time of Au was 1, 2 and 5 s, then obtained $Au_{(1s)}$-Pd_1Ni_4/RGO, $Au_{(2s)}$-Pd_1Ni_4/RGO and $Au_{(5s)}$-Pd_1Ni_4/RGO. $Au_{(x)}$-Pd_1Ni_4/RGO electrode can be used for electrochemical performance testing and SEM, EDX, TEM and XRD characterization.

Propane-1,3-diol oxidation was carried out in 0.5 mol L^{-1} NaOH solution containing 0.1 mol L^{-1} propane-1,3-diol on the $Au_{(x)}$-Pd_1Ni_4/RGO catalyst. After several potential cycles, stable cyclic voltammograms (CVs) were obtained. Oxygen of the electrolyte solutions was removed via Nitrogen gas of ultra-high purity. The electrochemical measurements were carried out at room temperature. All potentials were referred to SCE.

3. RESULTS AND DISCUSSION

3.1 Modification of Au on Pd_1Ni_4/RGO Electrode

The mass of Au on Pd_1Ni_4/RGO through the potentiostatic deposition in 1 mmol L^{-1} $HAuCl_4$ solution relied on the deposition time. The deposition of Au was performed for 1, 2 and 5 s by Pd_1Ni_4/RGO modified GCE (4 mm in diameter) corresponding to the charge of 10, 50 and 210 μC was obtained respectively. The positive potential of +0.60 V for a desired time was exerted on the GCE for the depositon of Au on Pd_1Ni_4/RGO was prepared in 0.05 mol·L^{-1} H_2SO_4 solution containing 1mmol L^{-1} $HAuCl_4$. The process has no hydrogen adsorption taken place on the Pd and Ni surface of Pd_1Ni_4/RGO. The Au deposits on the surface of the GCE obtained by the formula [$m = (Q \times M)/(Z \times F)$] are 0.16, 0.79 and 3.4μg cm^{-2} respectively. Where "m" is the metal mass, "Q" is the electric quantity, "M" is the relative atomic mass of the metal, "Z" is the metal charge converted into metal atom, "F" is the Faraday constant (9.65×10^4 C mol^{-1}). Since the Pd and Ni loading of Pd_1Ni_4/RGO is 2.5 μg. The corresponding Au/(Pd+Ni) atomic percentages of the prepared catalyst were 0.8, 4 and 17.2% respectively.

3.2 Characterization of Au-Pd_1Ni_4/RGO

The scanning electron microscopy (SEM) photograph of $Au_{(1s)}$-Pd_1Ni_4/RGO electrode surfaces are presented in Fig.1. It shows the metal nanoparticles are equally distributed on edges of RGO and

the basal planes have no come together as a group seriously. In the meantime, it was found that thin RGO folds overlapped each other [1]. In the preparation of Pd_1Ni_4/RGO samples, the Graphite oxide (GO) were obtained by ultrasonic stripping. GO is easily dispersed in water owing to a large number of oxygen-containing groups (-COOH, -OH,-O-) on the surface, meanwhile, these groups furnish binding sites for the anchoring precursor metal ions [28, 29]. When $NaBH_4$ was introduced to the mixed solution consisting of $Ni(NO_3)_2$, $Pd(NO_3)_2$ and GO. The palladium, nickel ions and GO were in situ restored to Pd, Ni nanoparticles and RGO sheets, and then the formed Pd and Ni nanoparticles are supported on RGO sheets. Moreover, the Pd and Ni nanoparticles can play the part of "spacers" to keep from RGO sheets restacking.

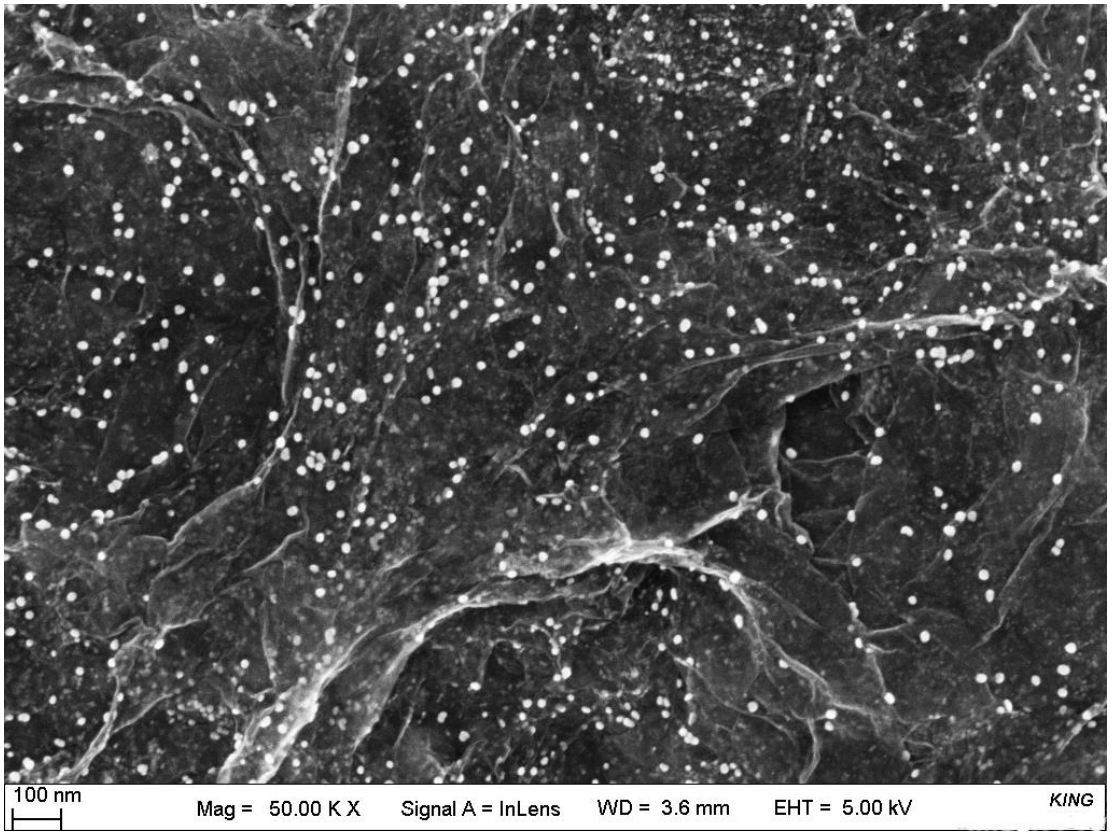

Figure 1. SEM images of $Au_{(1s)}$-Pd_1Ni_4/RGO electrode.

Fig. 2 displays the energy dispersive X-ray spectrum (EDX) of $Au_{(1s)}$-Pd_1Ni_4/RGO, and the peaks correspond to elements Ni, Au, Pd, C, O and Cl, indicating that nickel, gold and palladium exist in $Au_{(1s)}$-Pd_1Ni_4/RGO nanocomposites. The high intensity peak is assigned to carbon and oxygen, brought from GO. In addition, chlorine is considered to come from $HAuCl_4$.

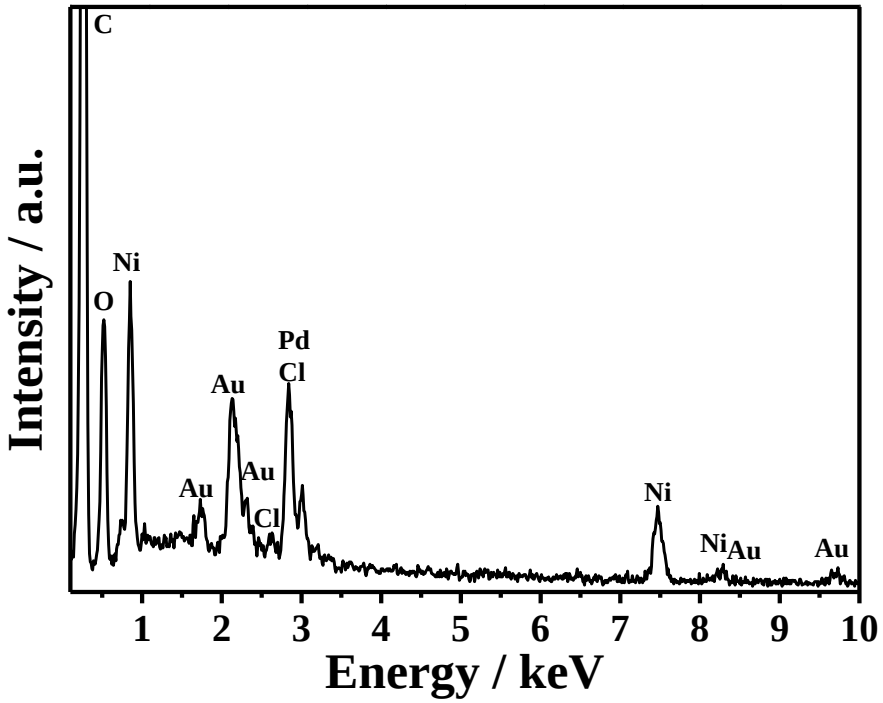

Figure 2. EDX images of $Au_{(1s)}$-Pd_1Ni_4/RGO electrode

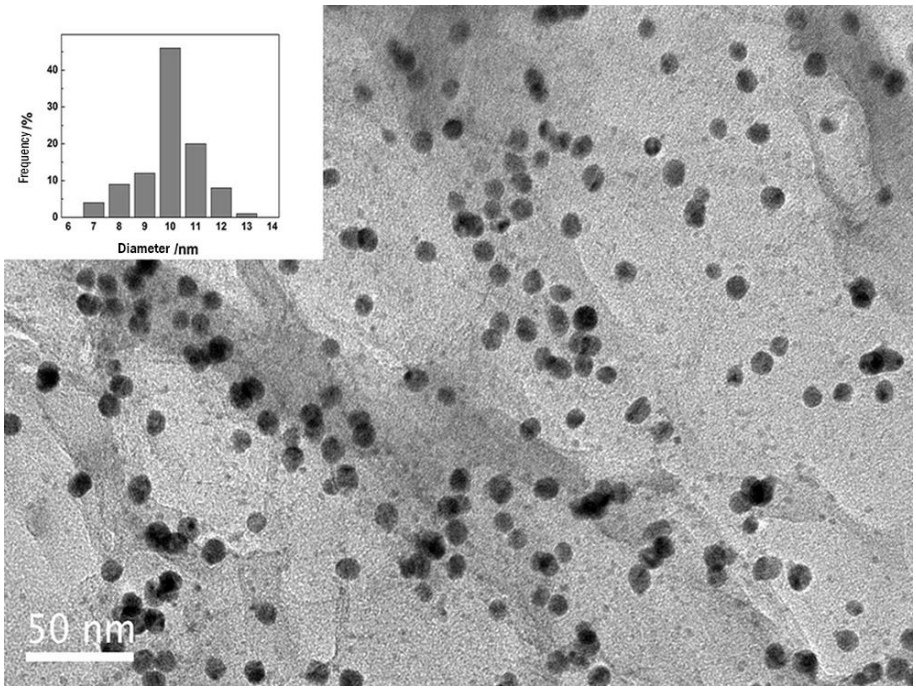

Figure 3 TEM images of $Au_{(1s)}$-Pd_1Ni_4/RGO electrode

The transmission electron microscopy (TEM) image of $Au_{(1s)}$-Pd_1Ni_4/RGO in Fig. 3. It is found that $Au_{(1s)}$-Pd_1Ni_4/RGO is composed of nanoparticles with different sizes from 7 to 13 nm, mainly in 10 and 11 nm. The average particle size is 9.97 nm via randomly selecting 100 particles. The particles

were homogeneously distributed on the RGO surface and edges without apparent agglomeration, which agree well with SEM.

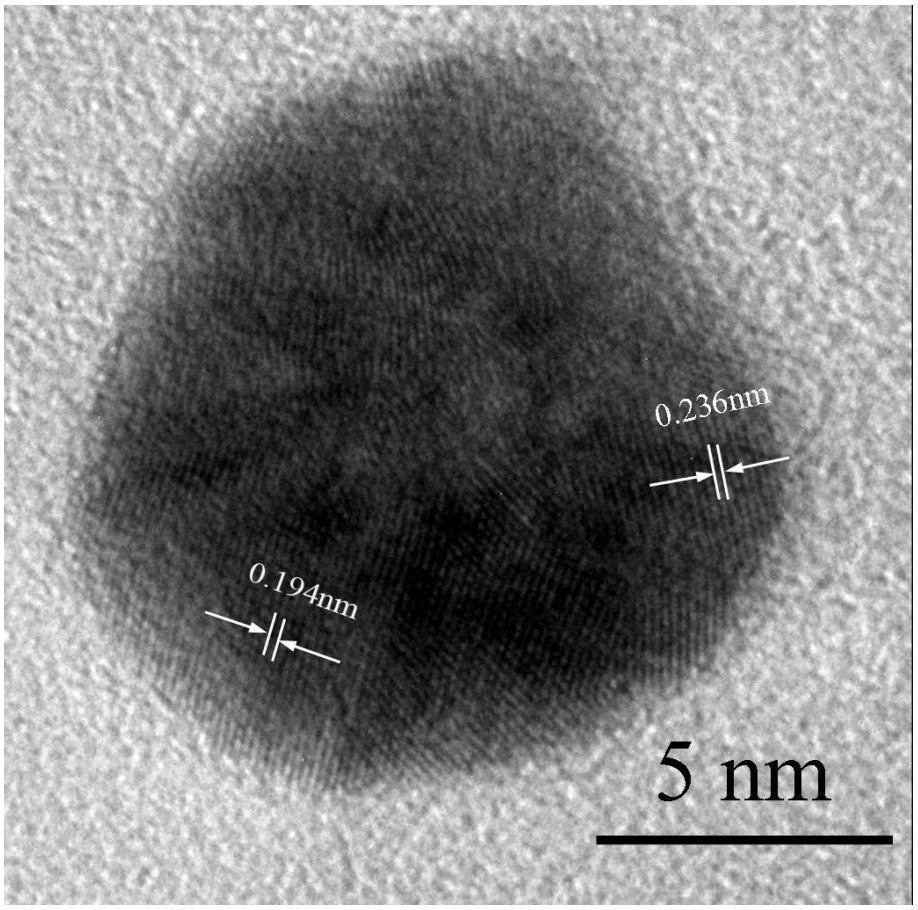

Figure 4. HRTEM images of $Au_{(1s)}$-Pd_1Ni_4/RGO electrode

Fig. 4 shows the high resolution transmission electron microscopy (HRTEM) image of an single nanoparticle. The single crystalline particle of $Au_{(1s)}$-Pd_1Ni_4/RGO are confirmed. The lattice planes with interlayer distance of 0.236 nm are indexed to Au (111) crystal planes (JCPDS 04-0784), and the lattice space of 0.194 corresponds to Pd (200) crystal planes (JCPDS 04-0784). On the other hand, it has not feature of crystalline structure in a large part of the surface, which was deemed to be Ni surface with an shapeless structure. In Fig. 5, The X-ray diffraction (XRD) pattern shows two peaks at 2θ value of 38.2^o and 46.6^o, corresponding to the Au (111) and Pd (200) crystal planes respectively. However, the peak of Ni crystal planes was not observed in XRD, which is good agreement with HRTEM. These final results suggest that the existence of Au and Pd are confirm, and the Ni nanoparticles are mostly amorphous in structure. In XRD, Ni has not diffraction peak for Ni nanotubes [30] was also reported. The wide reflection peak at a 2θ value of approximately 25^o is owing to the C (002) reflection of the out-of-order stacked RGO sheets [31].

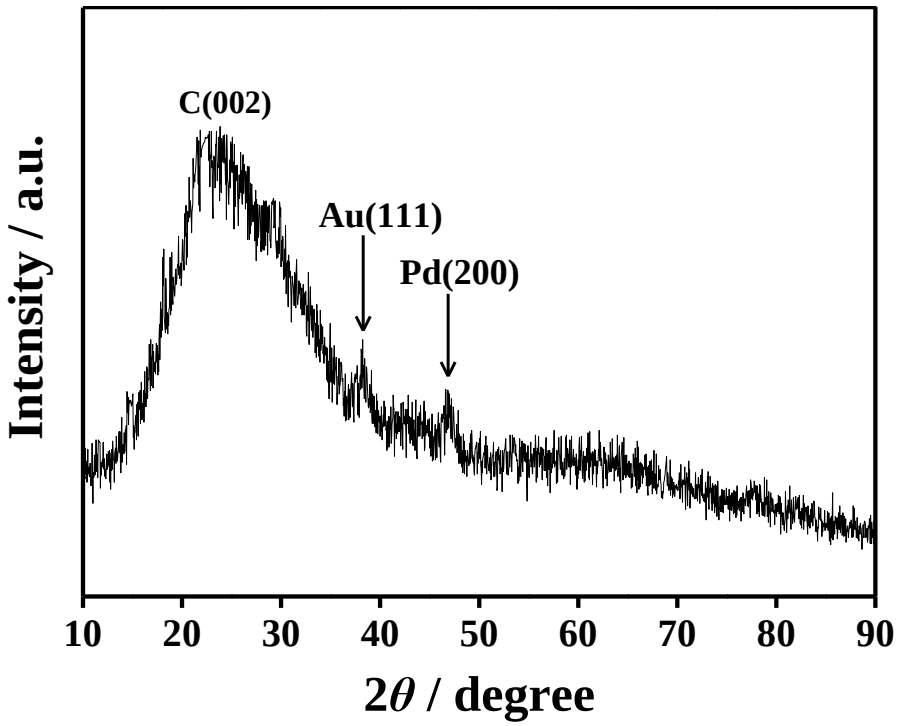

Figure 5. XRD images of $Au_{(1s)}$-Pd_1Ni_4/RGO electrode

3.3 Propane-1,3-diol oxidation of on $Au_{(x)}$-Pd_1Ni_4/RGO Electrode

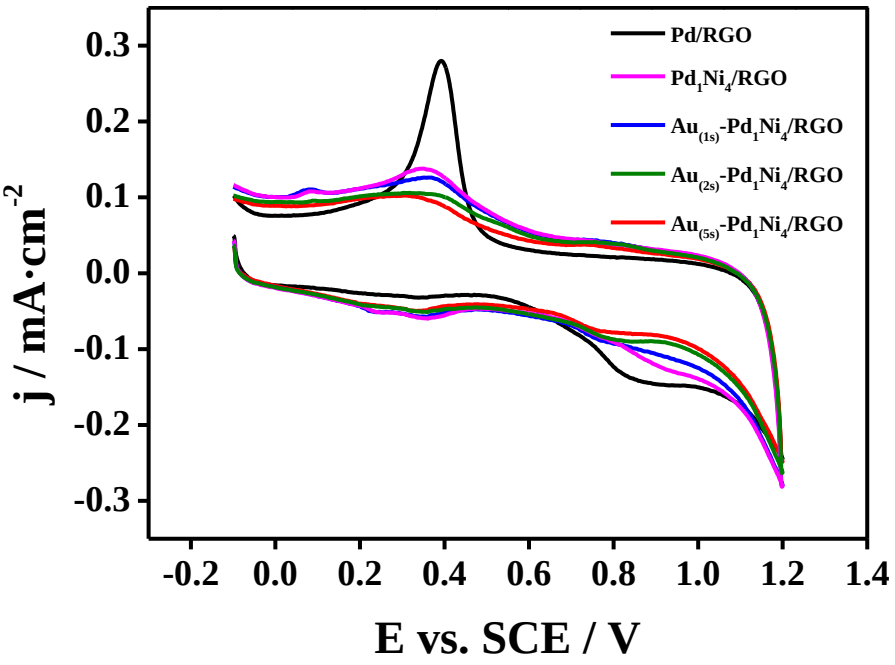

Figure 6. CVs of $Au_{(x)}$-Pd_1Ni_4/RGO, Pd_1Ni_4/RGO and Pd/RGO in 0.5 mol L^{-1} solution

Fig. 6 displays the cyclic voltammograms (CVs) of $Au_{(x)}$-Pd_1Ni_4/RGO, Pd_1Ni_4/RGO and Pd/RGO in sulfuric acid solution. Pd/RGO demonstrates a cathodic peak at +0.38 V, implying the

formation of palladium oxide reduction in the positive sweep clearly [20]. However, the $Au_{(x)}$-Pd_1Ni_4/RGO and Pd_1Ni_4/RGO displayed reduction peaks of palladium oxide much less than that on Pd/RGO. The current density of these peaks means a few of Au deposited. It could be seen that as the amount of Au deposition increases, these peak intensities decrease gradually. The peak integral charge of Pd after double correction is 424 μC cm^{-2} [4]. The Pd/RGO, Pd_1Ni_4/RGO, $Au_{(1s)}$-Pd_1Ni_4/RGO, $Au_{(2s)}$-Pd_1Ni_4/RGO and $Au_{(5s)}$-Pd_1Ni_4/RGO on GC substrates of 4 mm diameter demonstrated the electrochemically surface areas (ECSA) of Pd are 1.11, 0.35, 0.33, 0.21 and 0.11 cm^2 respectively.

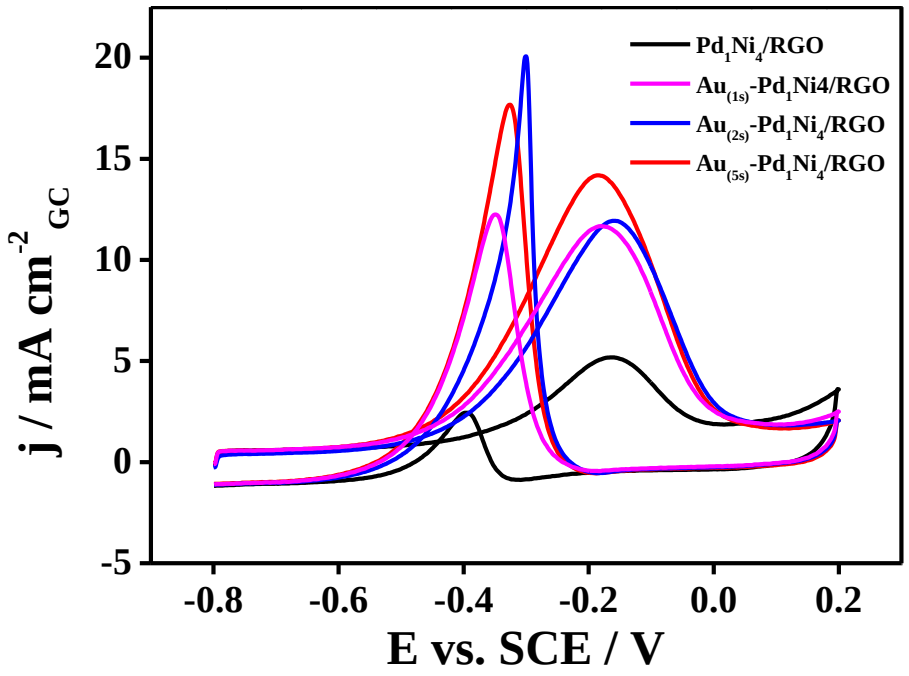

Figure 7. CVs of Pd_1Ni_4/RGO electrode and $Au_{(x)}$-Pd_1Ni_4/RGO electrode in 0.5 mol L^{-1} NaOH + 0.1 mol L^{-1} propane-1,3-diol. Current density is normalized to geometric surface area of GC substrate

Table 1. Cyclic voltammetry responses of the catalysts in 0.5 mol L^{-1} NaOH + 0.1 mol L^{-1} propane-1,3-diol[a]

Catalyst	E(V)[b]	*j*(mA cm^{-2})[c]
$Pt_{(0.28\%)}$/Ag/C	+0.76	10.1
$Pd_{0.25}/Au_{0.75}$/C	-0.15	17.5
$Au_{(20s)}$/Pd	-0.19	12.1
$Au_{(5s)}$-Pd_1Ni_4/RGO	-0.18	14.2

a Scan rate: 50mV s^{-1}; b Peak potential; c Peak current density.

Propane-1,3-diol oxidation on the $Au_{(x)}$-Pd_1Ni_4/RGO catalysts are recorded in Fig. 7, and the electrolyte consisted of 0.1 mol L^{-1} NaOH and 0.1 mol L^{-1} propane-1,3-diol. The peaks present different peak current densities at -0.18 V, but the peak positions and shapes are very similar to those

on Pd_1Ni_4/RGO. However, the $Au_{(x)}$-Pd_1Ni_4/RGO electrode exhibits a higher peak current density compare to the Pd_1Ni_4/RGO electrode. It is obvious that a small amount of Au precipitates can enhance the reaction kinetics of Pd_1Ni_4/RGO electrode and improve the electrocatalytic oxidation activity of propane-1,3-diol. As can be see, the peaks current density of Pd_1Ni_4/RGO, $Au_{(1s)}$-Pd_1Ni_4/RGO, $Au_{(2s)}$-Pd_1Ni_4/RGO and $Au_{(5s)}$-Pd_1Ni_4/RGO respectively are 5.2 mA cm^{-2}, 11.6 mA cm^{-2}, 12.1 mA cm^{-2} and 14.2 mA cm^{-2}. Furthermore, the peak current density of $Au_{(5s)}$-Pd_1Ni_4/RGO electrode reaches a maximum of about 3 times that of Pd_1Ni_4/RGO electrode, and the peak current density gradually increases with the increase of the amount of Au modification. The fact that a tiny amount of Au deposited on the surface of the Pd-Ni bimetallic particles increases the effective electrochemical active site of the electrode to show a better electrocatalytic oxidation performance. Then on the base of these, listed in Table 1 are previously works reported electrocatalytic oxidation of 1,3- propanediol compared to this work [20, 32]. We can see clearly from the Table 1 that the last one is the catalyst for this work this work. The electrocatalytic oxidation of 1,3- propanediol catalysts of $Pt_{(0.28\%)}$/Ag/C and $Au_{(20s)}$/Pd exhibited low peak current density(10.1 mA cm^{-2} and 12.1 mA cm^{-2}) compared to $Au_{(5s)}$-Pd_1Ni_4/RGO. Otherwise, $Pd_{0.25}/Au_{0.75}$/C showed higher peak current density(17.5 mA cm^{-2}) than catalyst for this work(14.2 mA cm^{-2}). From another point of view, $Pd_{0.25}/Au_{0.75}$/C cost higher than $Au_{(5s)}$-Pd_1Ni_4/RGO due to the more inexpensive Ni was doped in the composite, which reduced the amount of precious metals. In general, each catalyst has its own merits.

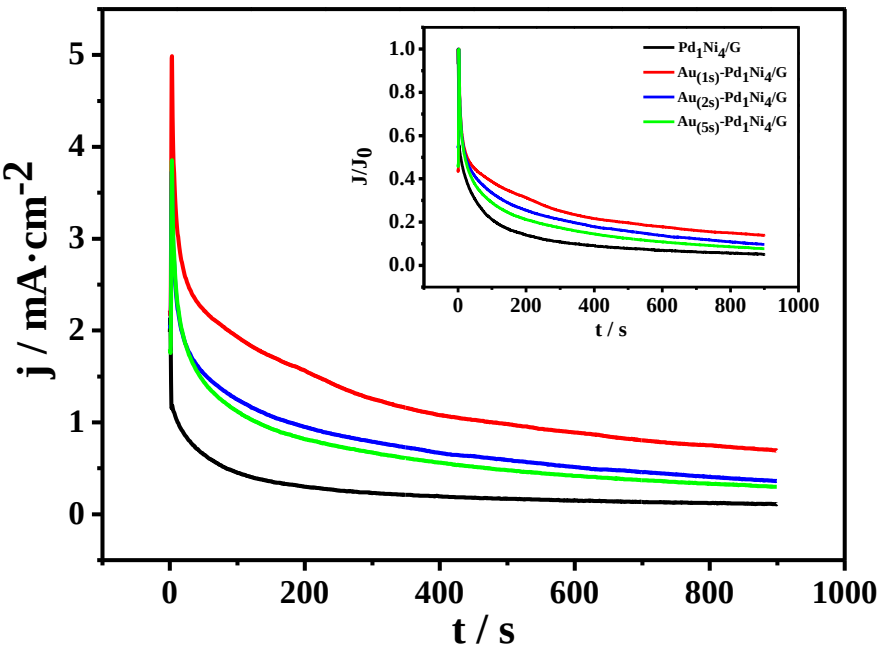

Figure 8. Chronoamperometric curves of Pd_1Ni_4/RGO and $Au_{(x)}$-Pd_1Ni_4/RGO in 0.5 mol L^{-1} NaOH + 0.1 mol L^{-1} propane-1,3-diol at a potential of -0.2 V.

The chronoamperometric curves of Pd_1Ni_4/RGO and $Au_{(x)}$-Pd_1Ni_4/RGO are shown in Fig. 8. It could be seen that the current density drops rapidly at the initial stage of the reaction due to the poisoning of Pd active sites by CO-like species. As the reaction progressed, the current density

decreased gradually and finally became steady. The inset of Fig. 8 plots the ratio of current density to maximum current density as ordinate. It could be seen from the inset, 95%, 86%, 90% and 92% current loss at the end of the reaction were observed for Pd_1Ni_4/RGO, $Au_{(1s)}$-Pd_1Ni_4/RGO, $Au_{(2s)}$-Pd_1Ni_4/RGO and $Au_{(3s)}$-Pd_1Ni_4/RGO, respectively. The result shows that $Au_{(1s)}$-Pd_1Ni_4/RGO not only has the best electrocatalytic oxidation activity, but also has the best anti-poisoning ability among these types of electrodes. As Changchun Jin [1, 33] reviewed, the loss of current density on Pt/Ag/C and Pt/C at the end of reaction (95% and 98%) in one work and the another work reported the current decay of 83.3%, 89.5%, 92.7%, 95.0% and 93.7% is observed for $Ag_{(1s)}$-Pt/C, $Ag_{(2s)}$-Pt/C, $Ag_{(5s)}$-Pt/C, $Ag_{(10s)}$-Pt/C and Pt/C catalysts, respectively. On the whole, only the $Ag_{(1s)}$-Pt/C catalyst show a little higher resistance than the catalyst of this work ($Au_{(1s)}$-Pd_1Ni_4/RGO) to the poisoning. However, the $Au_{(1s)}$-Pd_1Ni_4/RGO cost lower than $Ag_{(1s)}$-Pt/C due to the more inexpensive Ni was doped in the composite, which reduced the amount of precious metals.

4. CONCLUSIONS

To summarise, Au-deposited Pd_1Ni_4/RGO catalysts were prepared by electrochemically depositing small quantities of Au on Pd-Ni nanoparticles supported on RGO. Different loading amount of $Au_{(x)}$-Pd_1Ni_4/RGO electrodes were obtained by varying the experimental time. The FE-SEM and TEM characterization indicated that the metal particles were uniformly distributed on the $Au_{(1s)}$-Pd_1Ni_4/RGO electrode. The calculated average particle size was 9.97 nm. The electrooxidation of propnane-1,3-diol on Au(x)-Pd_1Ni_4/RGO in alkaline solution revealed that the Au(x)-Pd_1Ni_4/RGO catalysts have a higher activity than the Pd1Ni4/RGO catalysts, although the Au loading was very small. Meanwhile, the peak current density inecreases with the increase of Au deposition. The highly reactive form of Au(x)-Pd1Ni4/RGO is attributed to the synergistic effect that between Au and Ni and the high standard of RGO. The results show that catalysts own high activity by using base metal nanoparticles and very few precious metals. In other words, the method is of great significance because of its simple and economic performance. The key to preparing such a catalyst is the correct choice of base metal, second metal and support material.

ACKNOWLEDGEMENT
We are grateful for financial support from the Jiangsu Key Laboratory of Advanced Catalytic Materials and Technology, and the Advanced Catalysis and Green Manufacturing Collaborative Innovation Center.

References

1. C.C. Jin, C.C. Wan, J.H. Zhu, R.L. Dong, and Q.S. Huo, *J. Electrochem. Soc.*, 163 (2016) H848.
2. C. Bianchini, and P.K. Shen, *Chem. Rev.*, 109 (2009) 4183.
3. M.H. Shao, *J. Power Sources,*196 (2011) 2433.
4. M. Grden, M. Łukaszewski, G. Jerkiewicz, and A. Czerwinski, *Eletrochim. Acta,* 53 (2008) 7583.

5. U. Köler, J. Kumpers, and M. Ullrich, *J. Power Sources*, 105 (2002) 139.
6. C.Wang, Y. Zhong,W. Ren, Z. Lei, Z. Ren, J. Jia, and A. Jiang, *Appl. Surf. Sci.*, 254 (2008) 5649.
7. M.A. Abdel Rahim, R.M. Abdel Hameed, and M.W. Khalil, *J. Power Sources*, 134 (2004) 160.
8. I. Danaee, M. Jafarian, F. Forouzandeh, F. Gobal, and M.G. Mahjani, *Int. J. Hydrogen Energy*, 33 (2008) 4367.
9. S.Y. Shen, T.S. Zhao, J.B. Xu, and Y.S. Li, *J. Power Sources*, 195 (2010) 1001.
10. Z.L. Liu, X.H. Zhang, and L. Hong, *Electrochem. Commun.*,11 (2009) 925.
11. T.Yang, C.M.R. de Almeida, D. Ramasamy, and F.J.A. Loureiro, *J. Power Sources*, 269 (2014) 46.
12. A.M. Molenbroek, J.K. Norskov, and B.S. Clausen, *J. Phys. Chem. B.*,105 (2001) 5450.
13. T. Shobha, C.L. Aravinda, P. Bera, L.G. Devi, and S.M. Mayanna, *Mater. Chem. Phys.*, 80 (2003) 656.
14. S.H. Yan, L.Z. Gao, S.C. Zhang, S.C. Zhang, L.L. Gao, W.K. Zhang, and Y.Z. Li, *Int. J. Hydrogen Energy*, 38 (2013) 12838.
15. Q.G. He, W. Chen, S. Mukerjee, S.W. Chen, and F. laufek, *J. Power Sources*, 187 (2009) 298.
16. M. Simões, S. Baranton, and C. Coutanceau, *Appl. Catal., B*, 93 (2010) 354.
17. R. Larsen, S. Ha, J. Zakzeski, and R.I. Masel, *J. Power Sources*, 157 (2006) 78.
18. G.J. Zhang, Y.E. Wang, Y. Chen, Y.M. Zhou, Y.W. Tang, L.D. Lu, J.C. Bao, and T.H. Lu, *Appl. Catal., B*, 102 (2011) 614.
19. M. Simões, S. Baranton, and C. Coutanceau, *J. Phys. Chem. C*, 113 (2009) 13369.
20. C.C. Jin, Z.Y. Wang, and Q.S. Huo, *Ionics*, 21 (2015) 841.
21. N. Kakaki, J. Maiti, S.H. Lee, B. Viswanathan, and Y.S. Yoon, *Chem. Rev.*,114 (2014) 12397.
22. E. Antolini, and E.R. Gonzalez, *J. Power Sources*, 195 (2010) 3431.
23. A. Serov, and C. kwak, *Appl. Catal., B*, 97 (2010) 1.
24. Z.Y. Zhang, L. Xie, J. Qi, D.J. Chadderdon, and W.Z. Li, *Appl. Catal., B*, 136 (2013) 29.
25. M.E.M. Chbihi, D. Takky, F. Hahn, H. Huser, J.M. Léger, and C. Lamy, *J. Electroanal. Chem.*, 463 (1999) 63.
26. W.S. Hummers, and R.E. Offeman, *J. Am. Chem. Soc.*, 80 (1958) 1339.
27. N.I. Kovtyukhova, P.J. Ollivier, B.R. Martin, T.E. Mallouk, S.A. Chizhik, E.V. Buzaneva, and A.D. Gorchinskiy, *Chem. Mater.*, 11 (1999) 771.
28. Y. Li, L. Tang, and J. Li, *Electrochem. Commun.*, 11 (2009) 846.
29. Y.L. Hsin, K.C. Hwang, and C.T. Yeh, *J. Am. Chem. Soc.*, 129 (2007) 9999.
30. X. Li, M. Wang, Y. Ye, and K. Wu, *Mater. Lett.*, 108 (2013) 222.
31. J. Zhao, L. Zhang, T. Chen, H. Yu, L. Zhang, H. Xue, and H. Hu, *J. Phys. Chem. C*, 116 (2012) 21374.
32. C.C. Jin, J.J. Zhang, R.L. Dong, and Q.S. Huo, *Chem. Lett.*, 44 (2015) 194.
33. C.C. Jin, X.Y. Ma. J.J. Zhang, R.L. Dong, and Q.S. Huo, *Eletrochim. Acta*, 146 (2014) 533.